
Assessing Model Generalization in Vicinity

Yuchi Liu

Australian National University
yuchi.liu@anu.edu.au

Yifan Sun

Baidu
sunyf15@tsinghua.org.cn

Jingdong Wang

Baidu
wangjingdong@baidu.com

Liang Zheng

Australian National University
liang.zheng@anu.edu.au

Abstract

This paper evaluates the generalization ability of classification models on out-of-distribution test sets without depending on ground truth labels. Common approaches often calculate an unsupervised metric related to a specific model property, like confidence or invariance, which correlates with out-of-distribution accuracy. However, these metrics are typically computed for each test sample individually, leading to potential issues caused by spurious model responses, such as overly high or low confidence. To tackle this challenge, we propose incorporating responses from neighboring test samples into the correctness assessment of each individual sample. In essence, if a model consistently demonstrates high correctness scores for nearby samples, it increases the likelihood of correctly predicting the target sample, and vice versa. The resulting scores are then averaged across all test samples to provide a holistic indication of model accuracy. Developed under the vicinal risk formulation, this approach, named vicinal risk proxy (VRP), computes accuracy without relying on labels. We show that applying the VRP method to existing generalization indicators, such as average confidence and effective invariance, consistently improves over these baselines both methodologically and experimentally. This yields a stronger correlation with model accuracy, especially on challenging out-of-distribution test sets. The code for our work is available [here](#)¹.

1 Introduction

Because of the ubiquitous existence of distributional shifts in real-world systems, it is important to evaluate the generalization capacity of trained models on out-of-distribution (OOD) test data. In practical OOD scenarios, because obtaining test ground truths is expensive, model evaluation techniques that do not rely on test labeled are attracting increasing attention.

For this problem, unsupervised risk measurements are introduced that capture useful model properties, such as confidence and invariance. These measurements serve as indicators of a model’s generalization ability. Importantly, for a sample of interest without ground-truth, these methods compute a risk proxy *merely using this sample alone*. For example, [21] use the maximum Softmax value of a test sample itself as its confidence score, and show that once averaged over the OOD test set, it serves as a reliable indicator. The Effective Invariance score [11] is computed as the prediction consistency between this sample and its transformed version (*e.g.*, rotation and grey-scale). Because these indicators measure model properties that underpin its generalization ability, they generally exhibit fair correlation with the model’s out-of-distribution accuracy.

¹<https://github.com/liuyvchi/Vicinal-Risk-Rroxy>

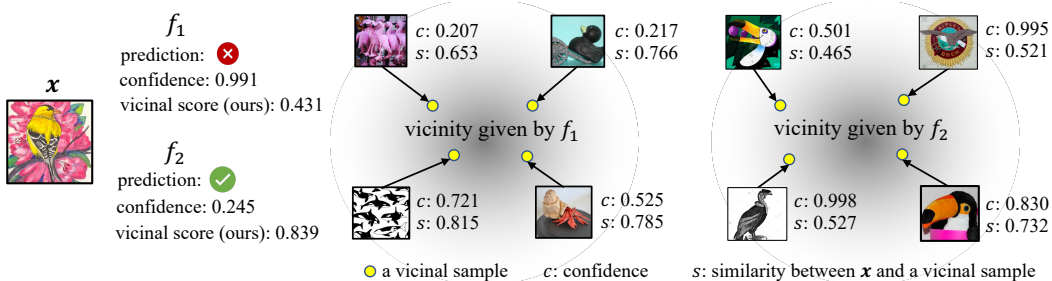


Figure 1: **Illustrating spurious model responses and how our method corrects them, we use confidence as a model generalization indicator.** For a given input x from ImageNet-R [22], models f_1 and f_2 incorrectly and correctly classify it, respectively. However, the confidence score (0.991) for the incorrect prediction by classifier f_1 is excessively higher than the score (0.245) for the correct prediction by classifier f_2 , indicating spuriousness. The model generalization ability ranking based on this test sample fails. Our proposed vicinal method, a similarity-weighted sum of confidence, provides more reasonable scores (0.431² and 0.839).

However, we find this isolated way of measuring model effectiveness for a sample of interest suffers from spurious model responses. In Fig. 1, we show two models where the one make incorrect prediction on a test sample may have a much higher confidence score than a model provide correct prediction. In other words, a high (*resp.* low) confidence or invariance score sometimes does not mean a correct (*resp.* incorrect) model prediction. These erroneous scores, once accumulated in the test set, would compromise the effectiveness of measuring (comparing) model risks.

To address this problem, when computing the risk proxy for a model on a test sample, we propose to integrate the risk proxy into the model behaviour on the adjacent samples, where such integration is performed using the vicinal distribution for the test sample (Fig. 1). Intuitively, if neighboring samples generally exhibit high risks (*e.g.*, low confidence), the center sample with excessively low risk will be assigned an increased risk score, and vice versa. Here, the contribution of each neighboring sample to the center sample is proportional to their similarity. This strategy allows model responses (risk proxy score) to better indicate model prediction correctness for the test sample, as shown at the bottom of Fig. 2. To indicate the overall generalization ability of models, we further compute the vicinal risk proxy (VRP) as the average individual vicinal score over the entire test set.

Another advantage of this vicinal assessment scheme is that it can be applied on top of various risk proxies based on individual test samples, including confidence, invariance and their variants. Our experiments show that VRP brings consistent improvements to them: stronger correlation between risk proxies rectified by VRP and model OOD accuracy over 200 different classifiers is generally observed on 9 benchmarks. In summary, this paper has the following main points.

- We examine existing methods in OOD generalization assessment in the lens of risk estimation.
- We propose to integrate vicinal distribution of a sample into its risk estimate, to inhibit spurious model responses.
- The proposed vicinal risk proxy (VPR), when applied to existing risk proxies, brings consistent improvement: stronger correlation is observed between vicinal proxies and model OOD accuracy.

2 Related Work

Data-centric model generalization assessment aims to predict the accuracy of a *given* model on *various* unlabeled test sets. Average model confidence [21, 35] on the testing samples is a simple and useful indicator of model accuracy. Guillory et al. [16] propose using the confidence discrepancy between the validation and test sets to correct the confidence-based accuracy. Deng et al. [10] tackle this challenge by comparing models based on their accuracy in self-supervised tasks. Garg et al. [15] predict accuracy by using the percentage of testing samples exceeding a threshold learned from a validation set in the source domain. In addition to confidence, domain shift can also be used as a cue

²We employ Eq. equation 11. For instance, the vicinal score of x in Fig. 1 is computed as: $0.431 = (0.653 \times 0.207 + 0.766 \times 0.217 + 0.815 \times 0.721 + 0.785 \times 0.525) / (0.653 + 0.766 + 0.815 + 0.785)$.

to predict model accuracy on the target set [16, 9]. This paper does not focus on this setup and only provides some results in the supplementary materials.

Model-centric generalization assessment. Some works focus on *in-distribution* generalization [14, 25, 30, 44]. This paper instead studies *OOD* generalization. In this problem, we train a variety of models on a training set and predict and compare their performance on an unlabeled *OOD* test set. Deng et al. [11] propose effective invariance (EI) to measure the consistency between model predictions on the original image and its transformed versions. It is also feasible to use data-centric indicators such as average confidence [21, 35]. However, we find these methods sometimes give excessively high (low) scores to incorrect (correct) samples, which compromise performance assessment; we show this problem can be alleviated by the proposed method.

Vicinal risk was originally introduced in the vicinal risk minimization (VRM) principle [5]. In VRM, each training sample defines a vicinal distribution, and accordingly, model risk is evaluated based on these distributions instead of individual training samples. VRM is widely reflected in data augmentation methods [5, 4, 31, 43, 40, 32, 27]. For example, MixUp [43] generates samples from vicinal distributions by mixing two images and their corresponding labels with random mixing weights. Other examples are CutMix [40], ResizeMix [32], and PuzzleMix [27]. While these methods reflect vicinal risks on labeled training data, we apply this idea to unlabeled test data. Our strategy smooths out spurious proxy scores and allows for better approximation to model out-of-distribution accuracy.

3 Preliminaries

3.1 Risk and Accuracy in Supervised Evaluation

We consider a model f belonging to a class of models \mathcal{F} and a target distribution $P(\mathbf{x}, y)$. Model risk can be formulated as the expectation of a given loss function $\ell(f(\mathbf{x}), y)$ on the distribution P during the test stage:

$$R(f) = \int \ell(f(\mathbf{x}), y) dP(\mathbf{x}, y). \quad (1)$$

In practice, since distribution $P(\mathbf{x}, y)$ is unknown, Eq. equation 1 cannot be directly computed. Standard practice thus approximates the test risk by replacing $P(\mathbf{x}, y)$ with an empirical distribution $P_{emp}(\mathbf{x}, y)$, formed by assembling Dirac delta functions [12] centered at each sample in a given test set $\mathcal{D} := \{(x_i, y_i)\}_{i=1}^n$:

$$dP_{emp}(\mathbf{x}, y) = \frac{1}{n} \sum_{i=1}^n \delta_{\mathbf{x}_i}(\mathbf{x}) \cdot \delta_{y_i}(y). \quad (2)$$

Substituting Eq. equation 2 into Eq. equation 1, the empirical risk under empirical target distribution P_{emp} becomes:

$$R_{emp}(f) = \frac{1}{n} \sum_{i=1}^n \ell(f(\mathbf{x}_i), y_i). \quad (3)$$

By convention, accuracy can be viewed as a type of empirical risk with the accuracy loss: $\ell_{acc} = 0$, if $\hat{y} = y$, otherwise $\ell_{acc} = 1$ where \hat{y} is the predicted class with maximum (Softmax) confidence in $f(\mathbf{x})$.

3.2 Vicinal Risk Minimization

In *training*, the risk (loss values) of individual *training* samples may not fairly reflect the true generalization ability of a model on this sample. That is, the model may trivially minimize $R_{emp}(f)$ in Eq. equation 3 by mere memorization of the samples [43, 42] rather than learn effective patterns. To address this problem, *vicinal risk minimization* [5] suggests to replace the Dirac delta function $\delta_{\mathbf{x}_i}(\mathbf{x})$ and $\delta_{y_i}(y)$ in Eq. equation 2 by some density estimates of the vicinity of point (\mathbf{x}_i, y_i) :

$$dP_v(\mathbf{x}, y) = \frac{1}{n} \sum_{i=1}^n dv(\mathbf{x}, y | \mathbf{x}_i, y_i), \quad (4)$$

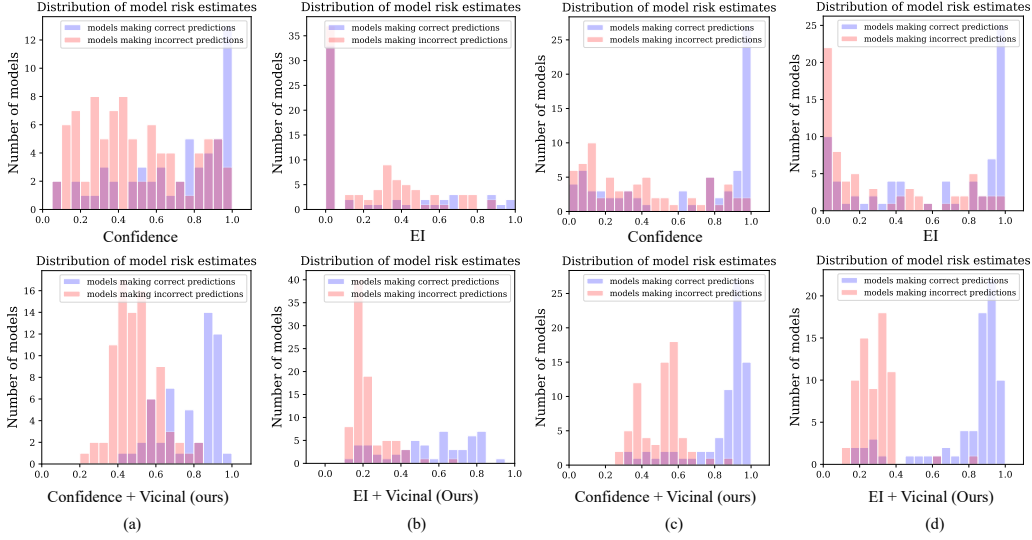


Figure 2: **Examples demonstrating how vicinal risks of individual samples can more efficiently differentiate between models making correct and incorrect predictions are provided.** In (a) - (b), a single test sample from ImageNet-R is used along with 140 models trained on the ImageNet training set. We employ risk estimates based on confidence[35, 21], confidence combined with our method, EI [11], and EI combined with our method. The distributions of these risk estimates across the 140 models for a given test sample are illustrated. In (c) - (d), results are reported for another test sample. Notably, confidence and EI, which rely on the sample in isolation, lead to spurious model responses. In the top row, many models making incorrect predictions may exhibit excessively high confidence/EI, while those making correct predictions may show unexpectedly low confidence/EI. In contrast, our method (bottom row)) effectively corrects these erroneous risk estimates, enhancing the separation of risk estimates on individual samples between good and poor models. Consequently, the vicinal risk proxy averaged over the entire out-of-distribution (OOD) test set becomes a more reliable indicator of model accuracy. **Additional examples are provided in the supplementary material (Fig. A1, A2 and A3), and further statistical results are presented in Fig 3.**

where $dv(\mathbf{x}, y|\mathbf{x}_i, y_i)$ is the vicinal density function describing the probability of finding point (\mathbf{x}, y) in the vicinity of (\mathbf{x}_i, y_i) , and P_v is a mixture distribution of n vicinal distributions v . The expectation of the vicinal risk of model f is now the mean of risk expectation in each vicinal distribution v :

$$R_v(f) = \int \ell(f(\mathbf{x}), y) dP_v(\mathbf{x}, y) = \frac{1}{n} \sum_{i=1}^n \int \ell(f(\mathbf{x}), y_i) dv(\mathbf{x}, y|\mathbf{x}_i, y_i). \quad (5)$$

The uniform vicinal distribution [5], Gaussian vicinal distribution [5] and mixup vicinal distribution [43] are well-known vicinity in the risk minimization task [41]. The success of vicinal risk minimization in *model training* [5, 4, 31, 18, 13, 43] demonstrates the effectiveness of this idea, which inspires us to enhance the risk estimation in the unsupervised *evaluation* problem.

4 Methodology

4.1 Risk Proxy in Unsupervised Evaluation

In unsupervised evaluation, it is infeasible to use ℓ_{acc} defined in Eq. equation 3 because of the absence of ground-truths. To still be able to indicate model risk, existing methods typically design a *proxy* loss $\hat{\ell}$ and compute its expectation on the unlabeled distribution $P(\mathbf{x})$:

$$\widehat{R}(f) = \int \hat{\ell}(f, \mathbf{x}, \varphi) dP(\mathbf{x}), \quad (6)$$

where $\widehat{R}(f)$ is defined as *risk proxy*. $\hat{\ell}$, usually reflecting crucial model properties (e.g., confidence and invariance), is computed based on the response of model f to input \mathbf{x} , and additional knowledge φ

of the model. In average confidence [35] and EI [11], $\hat{\ell}$ takes the confidence of \mathbf{x} or its transformation, so $\varphi = \emptyset$. In DoC [16], φ means model accuracy and average confidence evaluated on a validation set. In ATC [15], φ is a model-specific confidence threshold learned from a validation set.

In practice, on a test set with n test samples, $\widehat{R}(f)$ is approximated by the *empirical risk proxy*:

$$R_{emp}(f) = \frac{1}{n} \sum_{i=1}^n \hat{\ell}(f, \mathbf{x}_i, \varphi). \quad (7)$$

4.2 Proposed Vicinal Risk Proxy

Issues of empirical risk proxies. Existing methods in unsupervised evaluation assume that the designed risk proxy $\widehat{R}(f)$ well correlates with model generalization on the target OOD distribution. However, this assumption can be tenuous when we zoom in individual samples. As depicted at the top of Fig. 2, many models correctly classifying a sample have unexpected low confidence/invariance scores, and many incorrectly model predictions have excessively high confidence/invariance scores. The presence of such spurious model responses in individual samples introduces noise to the empirical risk proxy defined in Eq. equation 7, rendering it less effective in assessing model generalization capabilities. The dual problem in *training* is described in Section 3.2.

Solution. Given an unlabeled test set $\mathcal{D} := \{(\mathbf{x}_i)\}_{i=1}^n$, we propose to compute the *vicinal risk proxy* on \mathcal{D} as an unsupervised indicator of the accuracy of model f on this test set. We first define vicinal distribution μ for each test sample \mathbf{x}_i below:

$$\mu(\mathbf{x}, y | f, \mathbf{x}_i). \quad (8)$$

The probability density function for μ is defined as:

$$d\mu(\mathbf{x}, y | f, \mathbf{x}_i) = \begin{cases} s(f(\mathbf{x}^t), f(\mathbf{x}_i^t)), & \text{if } \hat{y}^t = \hat{y}_i^t, \\ 0, & \text{if } \hat{y}^t \neq \hat{y}_i^t, \end{cases} \quad (9)$$

where \mathbf{x}^t is a transformed view of \mathbf{x} , and \hat{y}_i^t is the predicted class of \mathbf{x}_i^t . There are various options for image transformations in practice (e.g., grayscale, color jitter, rotation, etc.), and we have empirically selected rotation for simplicity. The function $s(\cdot, \cdot)$ calculates the similarity between outputs generated by the model f , with the similarity computed empirically through the dot product³ of the Softmax vectors. Intuitively, μ is the probability distribution of finding pair (\mathbf{x}, y) in the vicinity of \mathbf{x}_i , and $d\mu$ is its probability density function. Integrating such vicinal assessment into the point-wise empirical risk proxy, Eq. equation 7 can be updated as the vicinal risk proxy:

$$\widehat{R}_v(f) = \frac{1}{n} \sum_{i=1}^n \int \hat{\ell}(f, \mathbf{x}, \varphi) d\mu(\mathbf{x}, y | f, \mathbf{x}_i). \quad (10)$$

Essentially, instead of merely using \mathbf{x}_i itself for risk estimation, we also use its neighboring samples. A sample with higher similarity with \mathbf{x}_i contributes more to the risk. We find that spurious model responses on \mathbf{x}_i can be effectively inhibited by its vicinal risks. For example, at the bottom of Fig. 2, for a test sample, models making correct and incorrect predictions are better separated. Quantitative analysis will be provided in Section 5.

In practice, we approximate the expectation of $\hat{\ell}$ within the i -th distribution μ as:

$$\mathbb{E}_i = \frac{\sum_{j=1}^{m_i} \hat{\ell}(f, \mathbf{x}_j, \varphi) d\mu(\mathbf{x}_j, \hat{y}_j | f, \mathbf{x}_i)}{\sum_{j=1}^{m_i} d\mu(\mathbf{x}_j, \hat{y}_j | f, \mathbf{x}_i)}, \quad (11)$$

where \hat{y}_j is the predicted class of \mathbf{x}_j in \mathcal{D} , and m_i is the number of vicinal samples in a vicinal distribution of \mathbf{x}_i ⁴. Intuitively, Eq. equation 11 gives an empirical estimation of the risk proxy

³We do not constrain the choice of the similarity metric in our method; however, for simplicity in our experiments, we opt for the dot product.

⁴By default, m_i is the count of samples with a probability density value greater than 0 in Eq. equation 9. Experiments illustrating the impact of m_i are presented in Fig. 5.

considering the vicinal distribution of x_i and the probability density defined in Eq. equation 9 for each vicinal sample. We provide the computational cost analysis for our method in Appendix C.

For individual samples, the vicinal score allows correct and incorrect model predictions to be better separated (refer Fig. 2 for an example). Collectively on the test set, models making more correct predictions (higher accuracy) will receive higher vicinal scores than models make less correct prediction (lower accuracy). An illustrative derivation is presented in Appendix for further clarity.

4.3 Apply Vicinal Risk Proxy to Existing Proxies.

In Eq. equation 6 and Eq. equation 7, we show that some existing approaches in unsupervised evaluation can be seen as unsupervised proxies for the empirical risk on the test set. Moreover, Eq. equation 10 means that the proposed vicinal risk proxy marries existing risk proxies with vicinal distribution. In other words, the idea of considering vicinal samples can be applied to various proxy loss functions $\hat{\ell}$. For example, when $\hat{\ell}$ is sample confidence, or equivalently, $\widehat{R}_{emp}(f)$ is the test average confidence [35, 21] computed empirically, also called empirical risk proxy (ERP). $\widehat{R}_v(f)$ is the the vicinal average confidence under our vicinal assessment, so is called vicinal risk proxy (VRP). By default, we search for neighboring samples for each vicinal distribution throughout the entire dataset. Samples with similarities greater than 0 are used to approximate the VRP score in Eq. equation 11. for this vicinity.

4.4 Discussions

Why do spurious model responses occur? Spurious model responses can occur for various reasons. One prominent factor is the over-confidence/under-confidence problem, as highlighted by Guo et al. [17] in their work on calibration. While model calibration can assist in alleviating this issue in in-distribution (IND) datasets, spurious model responses become inevitable in out-of-distribution (OOD) scenarios. Consequently, exploring effective solutions to assess model generalization while considering the negative impact of these spurious responses is an intriguing area.

Effectiveness of vicinal assessment under in-distribution test sets. For IND data, models generally have consistently good behaviours on test samples (including their neighbors, apparently). As such, considering the vicinity does not give additional knowledge. In fact, we empirically find that applying our method on IND data does not compromise the system (refer Table 1). Therefore, the proposed vicinal assessment is safe to use for both IND and OOD environments.

How can we guarantee neighborhood samples give correct responses? We do not assume this. Instead, we look at response consistency in the neighborhood. If the neighborhood responses are consistent with the center sample, the risk of the center sample is reliable; if responses are incorrect, the risk of the center sample would not be reliable and needs to be balanced by its vicinity responses.

Vicinal assessment for data-centric unsupervised evaluation. When we assume fixed classifier and training data and vary the test data [10, 15], technically vicinal assessment can be applied. However, the vicinal score of a single sample is only demonstrated to separate different *models* (see Fig. 2). In the date-centric scenario, it is not even possible to let a single sample separate different datasets, simply because different datasets do not share image samples. As such, we report that vicinal risk does not have noticeable improvement under the data-centric setup in the supplementary material.

Application to other risk proxies. The risk proxies considered in this paper, *e.g.*, EI [11] and AC [35, 21], are computed for individual samples. For model generalization analysis, some existing works are computed from the entire test set, such as ProjNorm [39], Dispersion Score [38] and COT [29]. We speculate that our method cannot be applied to these global scoring methods.

5 Experiments

5.1 Datasets and Evaluation Metrics

ImageNet-1k setup. 1. Model. We use 140 models that have been trained or fine-tuned using the ImageNet-1k [8] training set. We source these models from the models zoo Timm [37]. As suggested by Deng et al. [11], these models exhibit a diverse range of architectures, training strategies, and pre-

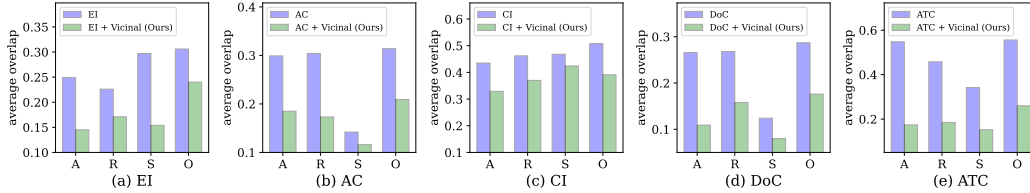


Figure 3: The average overlap of risk estimates for individual samples between correct and incorrect model predictions. We first estimate the distributions of risk estimate scores for correct and incorrect model predictions (140 in total) for each test sample. Then, the overlap of the two distributions for each sample is computed and finally averaged over the entire test set. All models are trained on ImageNet. In each figure, we use four test sets, ImageNet-A (A), ImageNet-R (R), ImageNet-S (S), and ObjectNet (O). From (a) to (e), EI, AC, CI, DoC, and ATC are used as baselines, respectively. *a smaller value indicates lower overlap or higher separability.* We clearly observe that vicinal risk scores (ours) statistically better differentiate models making correct and incorrect predictions by better separating their scores.

training settings. **2. Data.** (1) *ImageNet-A(dversarial)* [23] comprises natural adversarial examples that are unmodified and occur in the real-world. (2) *ImageNet-S(ketch)* [36] contains images with a sketch-like style. (3) *ImageNet-R(ention)* [22] comprises of 30,000 images that exhibit diverse styles. (4) *ImageNet-Blur* [20] was produced by applying a Gaussian function to blur the images from ImageNet-Val. We use blur with highest severity. (5) *ObjectNet* [2] is a real-world set for object recognition with control where object backgrounds, rotations, and imaging viewpoints are random. (6) *ImageNet-V2* [34] is a reproduced ImageNet dataset, whose distribution is similar to ImageNet.

CIFAR10 setup. **1. Model.** We use 101 models in this set sup. We follow Deng et al. [11] to access model weights. **2. Data.** (1) *CINIC-10* [7] is a fusion of CIFAR-10 and ImageNet-C [20] image classification datasets. It contains the same 10 classes as CIFAR-10. (2) *CIFAR-10.1* [33] is produced with almost the same distribution as CIFAR-10.

iWildCam setup. **1. Model.** We use 35 models trained on the iWildCam[3] training set. **2. Data.** iWildCam-OOD test set contains animal pictures captured in the wild.

Evaluation metrics. We use the same evaluation metrics as [11], *i.e.*, Pearson’s Correlation coefficient (γ) [6] and Spearman’s Rank Correlation coefficient (ρ) [26]. They assess the degree of linearity and monotonicity between risk proxies and OOD accuracy, respectively. The values of both coefficients fall between -1 and 1. A coefficient being close to -1 or 1 indicates a robust negative or positive correlation. Conversely, a value of 0 denotes no correlation [6]. Following [11], we use top-1 classification accuracy as a metric to measure model generalization.

5.2 Existing Risk Proxies as Baselines

We evaluate the effectiveness of vicinal assessment in enhancing the following risk proxies in unsupervised generalization prediction. 1) *Average Confidence* (AC) [35, 21]. The mean of the softmax confidence for each samples on the test set. 2) *Effective Insurance* (EI) [11] is the multiplication between the confidence of the image and a different view of it (*e.g.*, rotation) if the predicted class of them is the same. Otherwise, it is equal to zero for this sample. 3) *Consistency Invariance* (CI) [1] is the predicted probability of the transformed view affecting the predicted class of the original image. 4) *Difference of Confidence* (DoC) [16] is obtained by using the accuracy on the held-out validation set to subtract the gap between the AC on the validation set and the AC on the test set. 5) *Average Thresholded Confidence* (ATC) [15] quantifies the proportion of samples that have a softmax confidence score exceeding the threshold learned from the validation set.

5.3 Main Observations

Statistically, vicinal risk scores better differentiate correct and incorrect model predictions. In addition to the example in Fig. 2, we offer statistical evidence of our method’s functionality. We use Gaussian kernel density estimation (KDE) to estimate the distributions of proxy scores for models making correct and incorrect predictions on each sample. Subsequently, we employ numerical integration to calculate their overlap, known as the overlap coefficient. Fig. 3 presents the average

Table 1: **Comparing vicinal risk proxies (VRP) and empirical risk proxies (ERP) on various test sets.** For each test set, the first row shows ERP results, and the second row shows VRP results. γ and ρ represent the Pearson’s coefficient and the Spearman’s correlation coefficient, respectively. \clubsuit means near IND test sets. The figures in **blue bold** (**red bold**) indicate that the correlation coefficient of VRP is **higher** (**lower**) than that of ERP with statistical significance (p-value < 0.05) based on the two-sample t-test. Otherwise, their difference is not statistically significant.

Train	Test	EI		AC		CI		DoC		ATC	
		γ	ρ	γ	ρ	γ	ρ	γ	ρ	γ	ρ
ImageNet	ImageNet-A	0.882	0.645	0.581	0.464	0.856	0.617	0.877	0.761	0.851	0.436
		0.900	0.692	0.624	0.503	0.905	0.722	0.908	0.797	0.866	0.481
	ImageNet-R	0.914	0.814	0.736	0.625	0.873	0.729	0.898	0.862	0.937	0.887
		0.956	0.931	0.818	0.736	0.931	0.854	0.905	0.894	0.967	0.946
	ImageNet-S	0.893	0.853	0.742	0.711	0.868	0.820	0.911	0.919	0.948	0.915
		0.920	0.871	0.763	0.728	0.878	0.840	0.926	0.931	0.954	0.953
	ObjectNet	0.961	0.949	0.788	0.777	0.958	0.946	0.819	0.834	0.841	0.860
	0.975	0.972	0.838	0.814	0.969	0.962	0.849	0.868	0.857	0.876	
CIFAR10	ImageNet-Blur	0.870	0.831	0.711	0.730	0.824	0.793	0.781	0.776	0.882	0.867
		0.907	0.857	0.737	0.741	0.829	0.802	0.821	0.821	0.912	0.890
	ImageNet-V2 \clubsuit	0.889	0.884	0.609	0.501	0.882	0.870	0.982	0.979	0.993	0.990
		0.895	0.881	0.613	0.513	0.886	0.887	0.990	0.984	0.995	0.993
CIFAR10	CINIC	0.913	0.936	0.978	0.887	0.834	0.876	0.985	0.953	0.983	0.937
		0.954	0.956	0.979	0.889	0.875	0.929	0.985	0.956	0.982	0.942
iWildCam	CIFAR10.1 \clubsuit	0.886	0.905	0.982	0.972	0.804	0.811	0.992	0.985	0.991	0.982
		0.883	0.886	0.982	0.972	0.813	0.855	0.992	0.985	0.991	0.982
iWildCam	iWildCam-OOD	0.337	0.362	0.635	0.445	0.268	0.258	0.547	0.532	0.509	0.526
		0.402	0.393	0.655	0.495	0.208	0.180	0.556	0.592	0.518	0.595

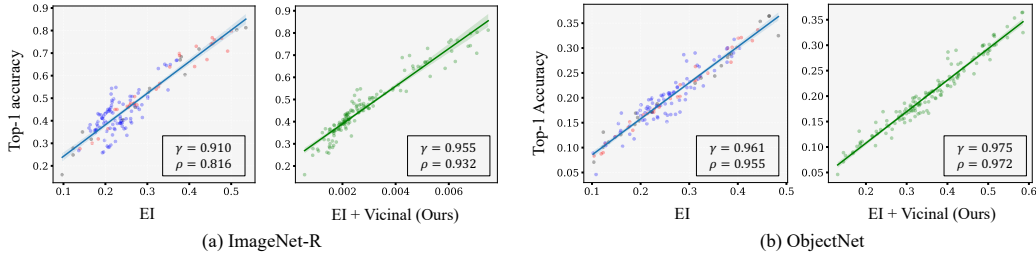


Figure 4: **Correlation between Effective Invariance (EI) and Accuracy:** Each dot in the figures represents a model, and straight lines are fitted using robust linear regression [24]. Blue dots represent the rectified score (VRP score) of these models, bringing their rank closer to the actual accuracy rank. Conversely, the rank of red models deviates further from the real accuracy when using the VRP paradigm. The rank of black models remains unchanged. The symbols ρ and γ have the same meaning as in Table 1. The shaded region in each figure represents a 95% confidence interval for the linear fit, calculated from 1,000 bootstrap samples. The VRP paradigm effectively rectifies the proxy score for the majority of models in both the ImageNet-R and ObjectNet datasets. Additional results for alternative risk proxies are presented in the supplementary material (Sec. F).

coefficient across each test set. The results illustrate that vicinal assessment yields a lower overlap coefficient compared to baseline proxies, facilitating the distinction between correct and incorrect predictions at the individual sample level.

Vicinal assessment consistently improves existing risk proxies on OOD test sets. In Table 1, we compare five existing risk proxies and their vicinal versions on OOD test sets. Each experiment is repeated three times to show statistical significance. We observe a consistent improvement in the strength of correlation between accuracy and risk proxy. For example, on ImageNet-A, vicinal assessment brings about 4.8%, 3.9%, 10.5%, 3.6%, and 4.5% improvement in the Spearman’s coefficient over EI, AC, CI, DoC, and ATC, respectively. These results indicate the effectiveness of the proposed method. The improvements can be illustrated by two examples in Fig. 4, where the ranks of the majority models have been adjusted to be closer to the actual rank.

Vicinal assessment is neither beneficial nor detrimental on near-OOD test sets. When test data are near OOD or even IND, the use of vicinal assessment does not have noticeable performance improvement or compromise. For example, on ImageNet-V2, we observe slight improvement for EI,

Table 2: **Comparison of variants of vicinal risk proxy. (Top)**: various similarity metrics that can be used in Eq. equation 9. **(Bottom)**: various image transformations that can be used in Eq. equation 9. Bold numbers denote the best one across compared settings.

Settings	EI		AC		CI		DoC		ATC	
	γ	ρ	γ	ρ	γ	ρ	γ	ρ	γ	ρ
Random	0.003	0.197	0.072	0.133	0.216	0.350	0.073	0.160	0.066	0.055
Equal	0.883	0.659	0.554	0.446	0.857	0.624	0.864	0.757	0.837	0.424
Gaussian kernel	0.876	0.675	0.611	0.498	0.887	0.706	0.887	0.797	0.881	0.532
Dot product	0.903	0.713	0.605	0.489	0.903	0.731	0.901	0.801	0.867	0.490
None	0.901	0.705	0.564	0.480	0.881	0.669	0.907	0.806	0.863	0.487
Grey-scale	0.898	0.686	0.617	0.503	0.879	0.655	0.917	0.812	0.889	0.514
Color jitters	0.897	0.674	0.632	0.512	0.861	0.642	0.919	0.811	0.874	0.482
Rotation	0.903	0.713	0.605	0.489	0.903	0.731	0.901	0.801	0.867	0.490

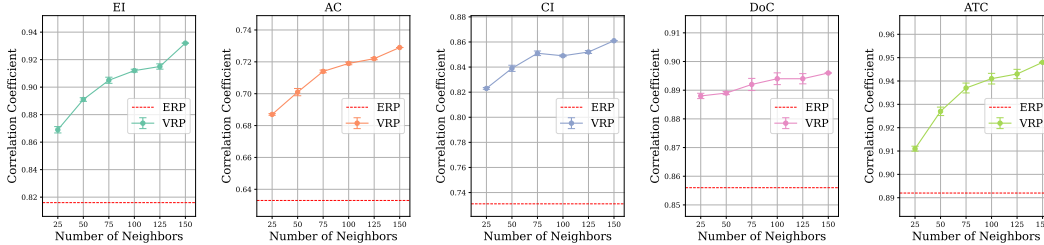


Figure 5: **Impact of the number of neighbors m on the correlation between proxy scores and accuracy.** We use five existing proxies as baselines and report the mean and standard deviation for each data point. We observe that vicinal assessment is consistently beneficial under various m values and yields stronger correlation with m increases.

CI, DoC and ATC, and slight decrease for AC. On the CIFAR10.1 test set, similar observations are made. Further given its effectiveness in OOD scenarios, this allows for safe deployment of vicinal assessment in practice.

5.4 Further Analysis of Vicinal Risk Proxy

Comparing different similarity measurements in Eq. equation 9. Dot product is used in Eq. equation 9 to compute similarity between a sample of interest and a sample in its vicinity. Here, we compare it with other options including random value (giving random similarity values), equal similarity (*i.e.*, uniform vicinal distribution [5]), and the Gaussian kernel function (*i.e.*, Gaussian vicinal distribution [5]). Results of ranking the 140 models on ImageNet-A are summarized in Table 2. We find that dot product generally has similar performance with Gaussian similarity, and both are much better than random similarity and equal similarity. It illustrates the benefit of letting closer sample to contribute more to the score of the sample of interest.

Comparing different image transformations. In Eq. equation 9, we define the probability density function for vicinal distribution using transformed images. Here we compare the effectiveness of different transformations, and results on ImageNet-A are presented in Table 2. We find that there is no significant performance difference between rotation, gray-scale transformation and color jitters.

Impact of the number of neighbors. The number of neighbors m is an important hyper-parameter used in Eq. equation 11. To evaluate system sensitivity to m , we experiment with ImageNet-R as OOD test set and five baseline risk proxies setting $m = 25, 50, 75, 100, 125, 150$ ⁵. We repeated each experiment three times and reported the mean and standard deviation. From Fig. 5 we have two observations. First, using more neighboring samples is generally beneficial, evidenced by the increasing correlation strength. It is probably because a larger m allows for better approximation of the true vicinal distribution. We set $m = 150$ by default. Second, when using fewer neighbors, *e.g.*, $m = 25$, vicinal assessment is still beneficial, yielding stronger correlation than existing risk proxies.

We provide further analysis, including discussions on time complexity, evaluation of variants, and the effects of test set size in Appendix C, D, and E, respectively.

⁵Because of the limited size of ImageNet-R, 150 is the maximum value we can set m to.

6 Conclusion

In this paper, we propose the vicinal assessment strategy to improve existing risk proxies computed based on a single test sample. We demonstrate that existing point-wise methods are prone to erroneous model responses, a problem that can be alleviated by considering the responses of adjacent test samples. Inspired by the philosophy of vicinal risk minimization, we design a vicinal risk proxy. We find that its computation on individual samples better differentiates models that make correct predictions from those that make incorrect ones. Therefore, when averaged across the test set, the vicinal risk proxy more accurately reflects the out-of-distribution (OOD) generalization ability of models. This main conclusion is verified through extensive experiments and further supported by analysis of its variants, sensitivity to key hyper-parameters, and application scope.

References

- [1] Sumukh Aithal, Dhruva Kashyap, and Natarajan Subramanyam. Robustness to augmentations as a generalization metric. *CoRR*, abs/2101.06459, 2021. 7
- [2] Andrei Barbu, David Mayo, Julian Alverio, William Luo, Christopher Wang, Dan Gutfreund, Josh Tenenbaum, and Boris Katz. Objectnet: A large-scale bias-controlled dataset for pushing the limits of object recognition models. *Advances in neural information processing systems*, 32, 2019. 7, 1
- [3] Sara Beery, Elijah Cole, and Arvi Gjoka. The iwildcam 2020 competition dataset. *arXiv preprint arXiv:2004.10340*, 2020. 7, 2
- [4] Yilong Cao and Peter I Rockett. The use of vicinal-risk minimization for training decision trees. *Applied Soft Computing*, 31:185–195, 2015. 3, 4
- [5] Olivier Chapelle, Jason Weston, Léon Bottou, and Vladimir Vapnik. Vicinal risk minimization. *Advances in neural information processing systems*, 13, 2000. 3, 4, 9
- [6] Israel Cohen, Yiteng Huang, Jingdong Chen, Jacob Benesty, Jacob Benesty, Jingdong Chen, Yiteng Huang, and Israel Cohen. Pearson correlation coefficient. *Noise reduction in speech processing*, pages 1–4, 2009. 7
- [7] Luke N Darlow, Elliot J Crowley, Antreas Antoniou, and Amos J Storkey. Cinic-10 is not imagenet or cifar-10. *arXiv preprint arXiv:1810.03505*, 2018. 7, 2
- [8] Jia Deng, Wei Dong, Richard Socher, Li-Jia Li, Kai Li, and Li Fei-Fei. Imagenet: A large-scale hierarchical image database. In *2009 IEEE conference on computer vision and pattern recognition*, pages 248–255. Ieee, 2009. 6, 1
- [9] Weijian Deng and Liang Zheng. Are labels always necessary for classifier accuracy evaluation? In *Proceedings of the IEEE/CVF conference on computer vision and pattern recognition*, pages 15069–15078, 2021. 3
- [10] Weijian Deng, Stephen Gould, and Liang Zheng. What does rotation prediction tell us about classifier accuracy under varying testing environments? In *International Conference on Machine Learning*, pages 2579–2589. PMLR, 2021. 2, 6
- [11] Weijian Deng, Stephen Gould, and Liang Zheng. On the strong correlation between model invariance and generalization. In *Advances in Neural Information Processing Systems*, 2022. 1, 3, 4, 5, 6, 7, 2
- [12] Paul Adrien Maurice Dirac. *The principles of quantum mechanics*. Number 27. Oxford university press, 1981. 3
- [13] Nanqing Dong, Jiayi Wang, and Irina Voiculescu. Revisiting vicinal risk minimization for partially supervised multi-label classification under data scarcity. In *Proceedings of the IEEE/CVF Conference on Computer Vision and Pattern Recognition*, pages 4212–4220, 2022. 4
- [14] Saurabh Garg, Sivaraman Balakrishnan, Zico Kolter, and Zachary Lipton. Ratt: Leveraging unlabeled data to guarantee generalization. In *International Conference on Machine Learning*, pages 3598–3609. PMLR, 2021. 3
- [15] Saurabh Garg, Sivaraman Balakrishnan, Zachary Chase Lipton, Behnam Neyshabur, and Hanie Sedghi. Leveraging unlabeled data to predict out-of-distribution performance. In *ICLR*, 2022. URL <https://arxiv.org/abs/2201.04234>. 2, 5, 6, 7
- [16] Devin Guillory, Vaishaal Shankar, Sayna Ebrahimi, Trevor Darrell, and Ludwig Schmidt. Predicting with confidence on unseen distributions. In *Proceedings of the IEEE/CVF International Conference on Computer Vision*, pages 1134–1144, 2021. 2, 3, 5, 7
- [17] Chuan Guo, Geoff Pleiss, Yu Sun, and Kilian Q Weinberger. On calibration of modern neural networks. In *International conference on machine learning*, pages 1321–1330. PMLR, 2017. 6
- [18] Luan Hai-Yan and Jiang Hua. Vicinal risk minimization based probability density function estimation algorithm using svm. In *2010 Third International Conference on Information and Computing*, volume 4, pages 161–164. IEEE, 2010. 4
- [19] Kaiming He, Xiangyu Zhang, Shaoqing Ren, and Jian Sun. Deep residual learning for image recognition. In *Proceedings of the IEEE conference on computer vision and pattern recognition*, pages 770–778, 2016. 2

- [20] Dan Hendrycks and Thomas Dietterich. Benchmarking neural network robustness to common corruptions and perturbations. *arXiv preprint arXiv:1903.12261*, 2019. 7, 1, 6
- [21] Dan Hendrycks and Kevin Gimpel. A baseline for detecting misclassified and out-of-distribution examples in neural networks. *Proceedings of International Conference on Learning Representations*, 2017. 1, 2, 3, 4, 6, 7
- [22] Dan Hendrycks, Steven Basart, Norman Mu, Saurav Kadavath, Frank Wang, Evan Dorundo, Rahul Desai, Tyler Zhu, Samyak Parajuli, Mike Guo, Dawn Song, Jacob Steinhardt, and Justin Gilmer. The many faces of robustness: A critical analysis of out-of-distribution generalization. *ICCV*, 2021. 2, 7, 1
- [23] Dan Hendrycks, Kevin Zhao, Steven Basart, Jacob Steinhardt, and Dawn Song. Natural adversarial examples. *CVPR*, 2021. 7, 1
- [24] Peter J. Huber. *Robust Statistics*, pages 1248–1251. Springer Berlin Heidelberg, Berlin, Heidelberg, 2011. ISBN 978-3-642-04898-2. doi: 10.1007/978-3-642-04898-2_594. URL https://doi.org/10.1007/978-3-642-04898-2_594. 8
- [25] Yiding Jiang, Vaishnavh Nagarajan, Christina Baek, and J Zico Kolter. Assessing generalization of sgd via disagreement. *arXiv preprint arXiv:2106.13799*, 2021. 3
- [26] Maurice George Kendall. Rank correlation methods. 1948. 7
- [27] Jang-Hyun Kim, Wonho Choo, and Hyun Oh Song. Puzzle mix: Exploiting saliency and local statistics for optimal mixup. In *International Conference on Machine Learning*, pages 5275–5285. PMLR, 2020. 3
- [28] Alex Krizhevsky, Geoffrey Hinton, et al. Learning multiple layers of features from tiny images. 2009. 2
- [29] Yuzhe Lu, Yilong Qin, Runtian Zhai, Andrew Shen, Ketong Chen, Zhenlin Wang, Soheil Kolouri, Simon Stepputtis, Joseph Campbell, and Katia Sycara. Characterizing out-of-distribution error via optimal transport. *arXiv preprint arXiv:2305.15640*, 2023. 6
- [30] Jeffrey Negrea, Gintare Karolina Dziugaite, and Daniel Roy. In defense of uniform convergence: Generalization via derandomization with an application to interpolating predictors. In *International Conference on Machine Learning*, pages 7263–7272. PMLR, 2020. 3
- [31] Ji Ni and Peter Rockett. Training genetic programming classifiers by vicinal-risk minimization. *Genetic Programming and Evolvable Machines*, 16:3–25, 2015. 3, 4
- [32] Jie Qin, Jiemin Fang, Qian Zhang, Wenyu Liu, Xingang Wang, and Xinggang Wang. Resizemix: Mixing data with preserved object information and true labels. *arXiv preprint arXiv:2012.11101*, 2020. 3
- [33] Benjamin Recht, Rebecca Roelofs, Ludwig Schmidt, and Vaishaal Shankar. Do cifar-10 classifiers generalize to cifar-10? 2018. <https://arxiv.org/abs/1806.00451>. 7, 2
- [34] Benjamin Recht, Rebecca Roelofs, Ludwig Schmidt, and Vaishaal Shankar. Do imagenet classifiers generalize to imagenet? In *International conference on machine learning*, pages 5389–5400. PMLR, 2019. 7, 1
- [35] Weijie Tu, Weijian Deng, Tom Gedeon, and Liang Zheng. Assessing model out-of-distribution generalization with softmax prediction probability baselines and a correlation method, 2023. URL <https://openreview.net/forum?id=1maXoEyeqx>. 2, 3, 4, 5, 6, 7
- [36] Haohan Wang, Songwei Ge, Zachary Lipton, and Eric P Xing. Learning robust global representations by penalizing local predictive power. In *Advances in Neural Information Processing Systems*, pages 10506–10518, 2019. 7, 1
- [37] Ross Wightman. Pytorch image models. <https://github.com/rwightman/pytorch-image-models>, 2019. 6, 1
- [38] Renchunzi Xie, Hongxin Wei, Yuzhou Cao, Lei Feng, and Bo An. On the importance of feature separability in predicting out-of-distribution error. *arXiv preprint arXiv:2303.15488*, 2023. 6
- [39] Yaodong Yu, Zitong Yang, Alexander Wei, Yi Ma, and Jacob Steinhardt. Predicting out-of-distribution error with the projection norm. In Kamalika Chaudhuri, Stefanie Jegelka, Le Song, Csaba Szepesvari, Gang Niu, and Sivan Sabato, editors, *Proceedings of the 39th International Conference on Machine Learning*, volume 162 of *Proceedings of Machine Learning Research*, pages 25721–25746. PMLR, 17–23 Jul 2022. 6

- [40] Sangdoon Yun, Dongyoon Han, Seong Joon Oh, Sanghyuk Chun, Junsuk Choe, and Youngjoon Yoo. Cutmix: Regularization strategy to train strong classifiers with localizable features. In *Proceedings of the IEEE/CVF international conference on computer vision*, pages 6023–6032, 2019. 3
- [41] Chao Zhang, Min-Hsiu Hsieh, and Dacheng Tao. Generalization bounds for vicinal risk minimization principle. *arXiv preprint arXiv:1811.04351*, 2018. 4
- [42] Chiyuan Zhang, Samy Bengio, Moritz Hardt, Benjamin Recht, and Oriol Vinyals. Understanding deep learning (still) requires rethinking generalization. *Communications of the ACM*, 64(3):107–115, 2021. 3
- [43] Hongyi Zhang, Moustapha Cisse, Yann N Dauphin, and David Lopez-Paz. mixup: Beyond empirical risk minimization. *arXiv preprint arXiv:1710.09412*, 2017. 3, 4
- [44] Lijia Zhou, Danica J Sutherland, and Nati Srebro. On uniform convergence and low-norm interpolation learning. *Advances in Neural Information Processing Systems*, 33:6867–6877, 2020. 3

A Experimental Setup

In this section, we introduce how to access the models and datasets used in our paper.

A.1 ImageNet Setup

Models. Following the practice of Deng et al. [11], we use the ImageNet models provided by PyTorch Image Models (timm) [37]. It provides models trained or fine-tuned on the ImageNet-1k training set [8]. We show the names of models used in our paper below:

'esmlp_36_224', 'cait_s36_384', 'cait_s24_224', 'convit_base', 'convit_tiny', 'twins_pcpvt_base', 'eca_nfnet_l1', 'xcit_tiny_24_p8_384_dist', 'efficientnet_b1', 'efficientnet_b3', 'efficientnet_b4', 'tf_efficientnet_b2', 'tf_efficientnet_lite1', 'convnext_base', 'convnext_small', 'resnetrs350', 'pit_xs_distilled_224', 'crossvit_small_240', 'botnet26t_256', 'tinynet_e', 'tinynet_d', 'repvgg_b2g4', 'mnasnet_small', 'dla46x_c', 'lcnet_050', 'tv_resnet34', 'tv_resnet50', 'tv_resnet101', 'tv_resnet152', 'densenet121', 'inception_v4', 'resnet26d', 'mobilenetv2_140', 'hrnet_w40', 'xception', 'xception41', 'resnet18', 'resnet34', 'seresnet50', 'mobilenetv2_050', 'seresnet33ts', 'wide_resnet50_2', 'wide_resnet101_2', 'resnet18d', 'hrnet_w18_small', 'gluon_resnet152_v1d', 'hrnet_w48', 'hrnet_w44', 'repvgg_b2', 'densenet201', 'hrnet_w18_small', 'resnet101d', 'gluon_resnet101_v1d', 'gluon_resnet101_v1s', 'gluon_xception65', 'gluon_seresnext50_32x4d', 'gluon_senet154', 'gluon_inception_v3', 'gluon_resnet101_v1c', 'tf_inception_v3', 'tv_densenet121', 'tv_resnext50_32x4d', 'repvgg_b1g4', 'resnext26ts', 'ghostnet_100', 'crossvit_9_240', 'deit_base_patch16_384', 'rexnet_150', 'rexnet_130', 'resnetrs50', 'resnet50d', 'resnet50', 'resnetv2_50', 'resnetrs152', 'resnetrs101', 'dpr92', 'dpr98', 'dpr68', 'vgg19_bn', 'vgg16_bn', 'vgg13_bn', 'vgg11_bn', 'vgg11', 'vgg11_bn', 'vgg16', 'vgg19', 'swin_small_patch4_window7_224', 'swin_base_patch4_window12_384', 'deit_base_patch16_224', 'deit_small_distilled_patch16_224', 'densenet161', 'tf_mobilenetv3_large_075', 'inception_v3', 'ssl_resnext101_32x8d', 'ssl_resnext101_32x16d', 'swsl_resnext101_32x8d', 'swsl_resnext101_32x16d', 'ssl_resnext101_32x4d', 'ssl_resnext50_32x4d', 'ssl_resnet50', 'swsl_resnext101_32x4d', 'swsl_resnext50_32x4d', 'swsl_resnet50', 'tf_efficientnet_l2_ns_475', 'tf_efficientnet_b7_ns', 'tf_efficientnet_b6_ns', 'tf_efficientnet_b4_ns', 'tf_efficientnet_b5_ns', 'convnext_xlarge_384_in22ft1k', 'convnext_xlarge_in22ft1k', 'convnext_large_384_in22ft1k', 'convnext_large_in22ft1k', 'convnext_base_384_in22ft1k', 'convnext_base_in22ft1k', 'resnetv2_152x2_bitm', 'resnetv2_152x4_bitm', 'resnetv2_50x1_bitm', 'resmlp_big_24_224_in22ft1k', 'resmlp_big_24_distilled_224', 'tf_efficientnetv2_s_in21ft1k', 'tf_efficientnetv2_m_in21ft1k', 'tf_efficientnetv2_l_in21ft1k', 'tf_efficientnetv2_xl_in21ft1k', 'vit_large_patch16_384', 'swin_large_patch4_window12_384', 'beit_large_patch16_512', 'beit_large_patch16_384', 'beit_large_patch16_224', 'beit_base_patch16_384', 'vit_base_patch16_384', 'vit_small_r26_s32_384', 'vit_tiny_patch16_384', 'vit_large_r50_s32_384', 'mixer_b16_224_miil', 'resmlp_big_24_224', 'resnetv2_50x1_bit_distilled', 'ig_resnext101_32x16d', 'ig_resnext101_32x32d', 'ig_resnext101_32x8d', 'ig_resnext101_32x48d', 'regnety_016', 'regnety_032'.

Datasets. We present the test sets employed in the main paper to evaluate the aforementioned ImageNet models. Datasets mentioned below can be accessed publicly via the provided links.

ImageNet-A(*adversarial*) [23]:

<https://github.com/hendrycks/natural-adv-examples>.

ImageNet-R(*rendition*) [22]:

<https://github.com/hendrycks/imagenet-r>.

ImageNet-Blur [20]:

<https://github.com/hendrycks/robustness>.

ImageNet-S(*sketch*) [36]:

<https://github.com/HaohanWang/ImageNet-Sketch>.

ImageNet-V2 [34]:

<https://github.com/modestyachts/ImageNetV2>.

ObjectNet [2]:

<https://objectnet.dev/download.html>.

A.2 CIFAR10 Setup

Models. We employ 101 models trained on the CIFAR10 training set. Among them, 82 are trained based on the implementation from <https://github.com/kuangliu/pytorch-cifar>, following the practice of Deng et al. [11]. These models vary in their architectures and number of training epochs. Specifically, the following architectures are used:

‘DenseNet121’, ‘DenseNet169’, ‘DenseNet201’, ‘DenseNet161’, ‘densenet_cifar’, ‘DLA’, ‘SimpleDLA’, ‘DPN26’, ‘DPN92’, ‘EfficientNetB0’, ‘GoogLeNet’, ‘LeNet’, ‘MobileNet’, ‘MobileNetV2’, ‘PNASNetA’, ‘PNASNetB’, ‘PreActResNet18’, ‘PreActResNet34’, ‘PreActResNet50’, ‘PreActResNet101’, ‘PreActResNet152’, ‘RegNetX_200MF’, ‘RegNetX_400MF’, ‘RegNetY_400MF’, ‘ResNet18’, ‘ResNet34’, ‘ResNet50’, ‘ResNet101’, ‘ResNet152’, ‘ResNeXt29_2x64d’, ‘ResNeXt29_4x64d’, ‘ResNeXt29_8x64d’, ‘ResNeXt29_32x4d’, ‘SENet18’, ‘ShuffleNetG2’, ‘ShuffleNetG3’, ‘ShuffleNetV2’, ‘VGG11’, ‘VGG13’, ‘VGG16’, ‘VGG19’.

For each architecture, we train two variants with 30 and 50 training epochs, respectively.

The rest 19 models are download from <https://github.com/cheneafo/pytorch-cifar-models>. Names of these models are listed below:

‘cifar10_mobilenetv2_x0_5’, ‘cifar10_mobilenetv2_x0_75’, ‘cifar10_mobilenetv2_x1_0’, ‘cifar10_mobilenetv2_x1_4’, ‘cifar10_repvvg_a0’, ‘cifar10_repvvg_a1’, ‘cifar10_repvvg_a2’, ‘cifar10_resnet20’, ‘cifar10_resnet32’, ‘cifar10_resnet44’, ‘cifar10_resnet56’, ‘cifar10_shuffleNetv2_x0_5’, ‘cifar10_shuffleNetv2_x1_0’, ‘cifar10_shuffleNetv2_x1_5’, ‘cifar10_shuffleNetv2_x2_0’, ‘cifar10_vgg11_bn’, ‘cifar10_vgg13_bn’, ‘cifar10_vgg16_bn’, ‘cifar10_vgg19_bn’.

Datasets. Datasets used in the CIFAR10 setup can be found through the following links.

CIFAR10 [28]:

<https://www.cs.toronto.edu/kriz/cifar.html>.

CIFAR10.1 [33]:

<https://github.com/modestyachts/CIFAR-10.1>.

CINIC [7]:

<https://github.com/BayesWatch/cinic-10>.

A.3 iWildCam Setup

Models. We access 34 models trained on the iWildCam training set from the official implementation of the iWildCam benchmark (<https://worksheets.codalab.org/worksheets/0x52cea64d1d3f4fa89de326b4e31aa50a>). All models use Resnet50 [19] as the backbone but differ in training algorithms, learning rate, weight decay, etc. Their identification names are provided below.

‘iwildcam_afn_extraunlabeled_tune0’, ‘iwildcam_dann_coarse_extraunlabeled_tune0’, ‘iwildcam_deepcoral_coarse_extraunlabeled_tune0’, ‘iwildcam_deepcoral_coarse_singlepass_extraunlabeled_tune0’, ‘iwildcam_deepCORAL_seed0’, ‘iwildcam_deepCORAL_seed1’, ‘iwildcam_deepCORAL_seed2’, ‘iwildcam_deepCORAL_tune’, ‘iwildcam_ermaugment_tune0’, ‘iwildcam_ermoracle_extraunlabeled_tune0’, ‘iwildcam_erm_seed0’, ‘iwildcam_erm_seed1’, ‘iwildcam_erm_seed2’, ‘iwildcam_erm_tune0’, ‘iwildcam_erm_tuneA_seed0’, ‘iwildcam_erm_tuneB_seed0’, ‘iwildcam_erm_tuneC_seed0’, ‘iwildcam_erm_tuneD_seed0’, ‘iwildcam_erm_tuneE_seed0’, ‘iwildcam_erm_tuneF_seed0’, ‘iwildcam_erm_tuneG_seed0’, ‘iwildcam_erm_tuneH_seed0’, ‘iwildcam_fixmatch_extraunlabeled_tune0’, ‘iwildcam_groupDRO_seed0’, ‘iwildcam_groupDRO_seed1’, ‘iwildcam_groupDRO_seed2’, ‘iwildcam_irm_seed0’, ‘iwildcam_irm_seed1’, ‘iwildcam_irm_seed2’, ‘iwildcam_irm_tune’, ‘iwildcam_noisystudent_extraunlabeled_seed0’, ‘iwildcam_pseudolabel_extraunlabeled_tune0’, ‘iwildcam_swav30_ermaugment_seed0’.

Dataset. *iWildCam-OOD* [3] can be download from the the official guidance: <https://github.com/p-lambda/wilds/>.

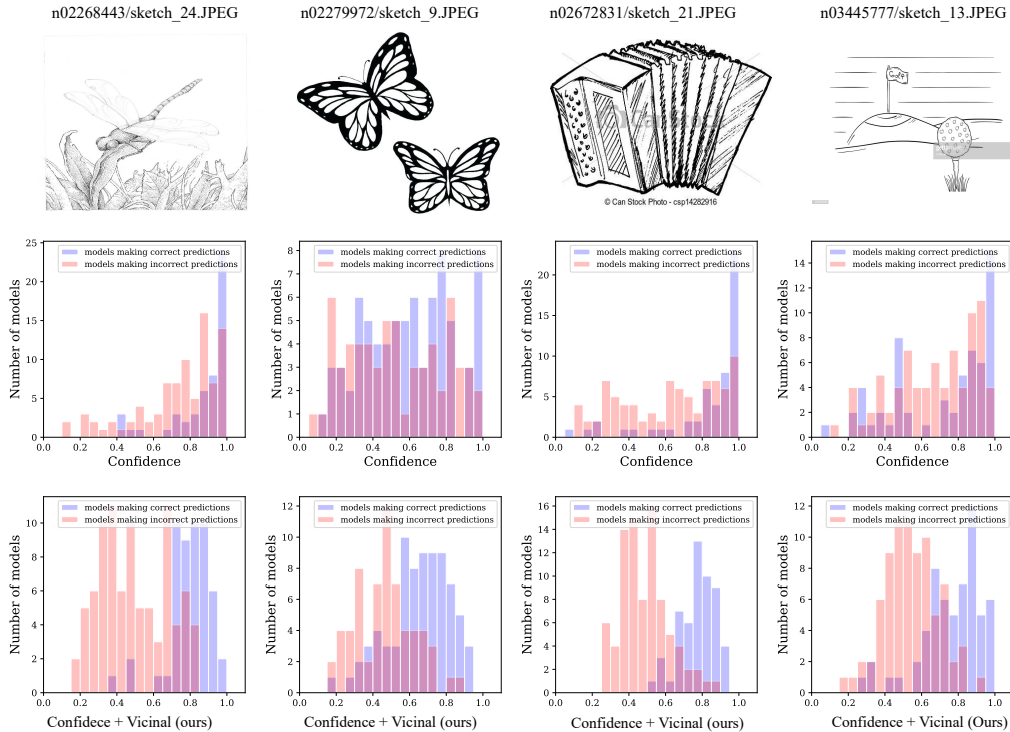


Figure A1: **Illustration of working mechanism of vicinal assessment on individual samples from ImageNet-S.** Four test samples are shown in the top row. The AC method is used as baseline proxy. Score distribution of 140 models trained on the ImageNet training set are drawn below. Notations have the same meaning as Fig. 2 in the main paper.

B Working Mechanism from Individual Test Samples to A Whole Test Set

As discussed in the working mechanism part (see Section 4.2 of the main paper), we attribute the effectiveness of our method to its ability to distinguish correct and incorrect model predictions on an individual sample level, and thus better separability of models with different OOD performance. In addition to the example shown in Fig. 2 of the main paper, we provide more examples to demonstrate the working mechanism on individual test samples in Fig. A1, Fig. A2, and Fig A3. We clearly observe that the distributions of model risk estimates of incorrect and correct predictions are generally more spreadable by using proposed vicinal assessment. These examples further showcase the working mechanism, where samples in the vicinity effectively rectify erroneous risk estimates, so that risk estimates of individual samples better differentiate models making correct and incorrect predictions. The advantage of our method exhibited on individual test samples can guarantee a successful model ranking across the entire dataset. Here is the derivation.

Definitions. There are two models, f_a , and f_b , to test. We denote each test sample in the test set as $\mathbf{x}_i, i \in \{1, 2, \dots, n\}$. Given an baseline empirical risk proxy \widehat{R}_e (e.g., AC, EI, and DoC), the empirical risk score of model f_a on the test sample \mathbf{x}_i is written as $\widehat{R}_e(f_a, \mathbf{x}_i)$. Similarly, the vicinal risk score of f_a in the vicinity of \mathbf{x}_i can be written as $\widehat{R}_v(f_a, \mathbf{x}_i)$. We assume f_a has higher accuracy than f_b and the risk proxy score is positively related to the model accuracy. Here, We define p_e^i as the probability of the event that the empirical risk score for f_a on the test sample \mathbf{x}_i is higher than that for f_b , where

$$p_e^i = P((\widehat{R}_e(f_a, \mathbf{x}_i) - \widehat{R}_e(f_b, \mathbf{x}_i)) > 0).$$

Similarly, we have

$$p_v^i = P((\widehat{R}_v(f_a, \mathbf{x}_i) - \widehat{R}_v(f_b, \mathbf{x}_i)) > 0),$$

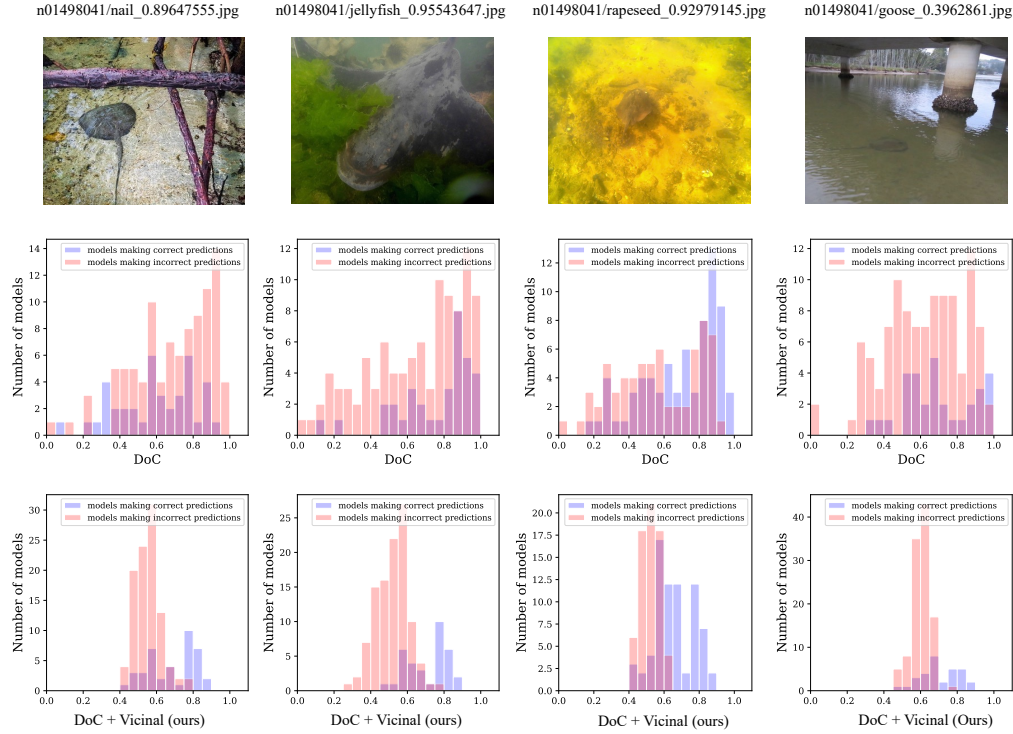


Figure A2: **Illustration of working mechanism of vicinal assessment on individual samples from ImageNet-A.** DoC is used as baseline proxy. Other notations have the same meaning as Fig. A1.

which means that the vicinal risk score for f_a on the test sample \mathbf{x}_i is higher than that for f_b .

Working mechanism. Given the preliminary assumption that the vicinal risk proxy \widehat{R}_v enables the score distributions of correct and incorrect model predictions for each test sample to be more separable than the empirical risk proxy \widehat{R}_e (shown by our experiments in Fig. 3 of the main paper), there are some arbitrary samples $\{\mathbf{x}_i\}, i \in \{1, 2, \dots, m\}, m \leq n$, where

$$p_v^i > p_e^i, \forall i \in \{1, 2, \dots, m\}.$$

In other words,

$$\begin{aligned} &P((\widehat{R}_v(f_a, \mathbf{x}_i) - \widehat{R}_v(f_b, \mathbf{x}_i)) > 0) \\ &> P((\widehat{R}_e(f_a, \mathbf{x}_i) - \widehat{R}_e(f_b, \mathbf{x}_i)) > 0), \forall i \in \{1, 2, \dots, m\}. \end{aligned}$$

Therefore, we have the following probability inequality:

$$\begin{aligned} &P\left(\left(\frac{1}{m} \sum_i^m \widehat{R}_v(f_a, \mathbf{x}_i) - \frac{1}{m} \sum_i^m \widehat{R}_v(f_b, \mathbf{x}_i)\right) > 0\right) > \\ &P\left(\left(\frac{1}{m} \sum_i^m \widehat{R}_e(f_a, \mathbf{x}_i) - \frac{1}{m} \sum_i^m \widehat{R}_e(f_b, \mathbf{x}_i)\right) > 0\right). \end{aligned}$$

According to Eq. 10 in the main paper, the above inequality can be rewritten as

$$P((\widehat{R}_v(\widehat{f}_a) - \widehat{R}_v(\widehat{f}_b)) > 0) > P((\widehat{R}_e(\widehat{f}_a) - \widehat{R}_e(\widehat{f}_b)) > 0),$$

where $\widehat{R}_v(\widehat{f}_a)$ and $\widehat{R}_v(\widehat{f}_b)$ are the vicinal score and the empirical risk score for model f_a , respectively. It means that our method has the higher probability to successfully rank models f_a and f_b .

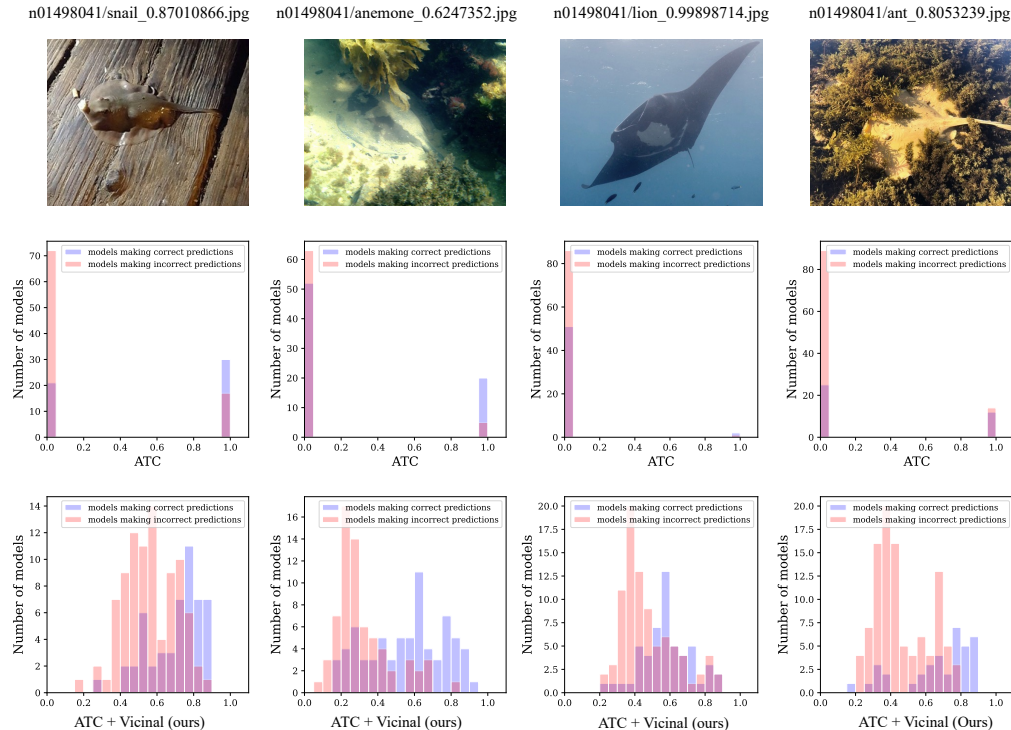


Figure A3: **Illustration of working mechanism of vicinal assessment on individual samples from ImageNet-R.** ATC is used as baseline proxy. Other notations have the same meaning as Fig. A1.

Table C1: Running time (seconds) vs. test set size (the whole test set) for average confidence (AC) and our method (AC+VRP). The last row presents the runtime increase caused by applying VRP to AC.

Test set size	5,000	10,000	15,000	20,000	25,000	30,000
AC (sec.)	1.75	1.88	1.95	1.99	2.14	2.22
AC + VRP (sec.)	4.38	4.57	4.76	5.02	5.23	5.40
Added time (sec.)	2.63	2.69	2.81	3.03	3.09	3.18

C Time Complexity

The computational complexity of our method is $O(nm)$, where n is test set size, and m is the number of neighboring samples used for VRP computation. In our algorithm, neighboring samples are those sharing the same predicted label as the sample of interest, so looking for neighboring samples does not require a search process. In our implementation, m is a hyperparameter that can be as small as 25 or 50 (see Fig. 6) to yield improvement, while a test sample may have 150 neighbors. So the computational complexity is much less than $O(n^2)$.

We would like to present the experimental results of time consumption under different dataset sizes here. In Table C1, we provide the running time of evaluating the model ‘vit_large_r50_s32_384’ on the ImageNet-R dataset. We used NVIDIA28 V100 with $4 \times$ GPU.

Two main observations can be drawn from the above table. First, compared with the baseline average confidence (AC) method, applying VRP (AC+VRP) consumes an additional 2-4 seconds when the test set size is 30k.

Second, the runtime of VRP increases almost linearly with the test set size. For example, VRP runtime increases by 1.02 seconds and when the test set size increases from 5k to 30k.

Table D2: **Comparison of variants of vicinal risk proxy on ImageNet-R (Top) and ObjectNet (Bottom)**. Notations follow Tab. 2 of the main submission.

Settings	EI		AC		CI		DoC		ATC	
	γ	ρ	γ	ρ	γ	ρ	γ	ρ	γ	ρ
Random (to do)	0.335	0.399	0.277	0.331	0.415	0.466	0.237	0.461	0.357	0.563
Equal	0.910	0.816	0.738	0.633	0.868	0.731	0.897	0.856	0.935	0.892
Dot product	0.955	0.932	0.817	0.729	0.925	0.861	0.909	0.896	0.966	0.948
None	0.816	0.743	0.704	0.606	0.874	0.731	0.889	0.825	0.894	0.786
Grey-scale	0.945	0.922	0.816	0.756	0.944	0.891	0.901	0.901	0.971	0.951
Color jitters	0.930	0.899	0.813	0.748	0.941	0.889	0.880	0.886	0.969	0.947
Rotation	0.955	0.932	0.817	0.729	0.925	0.861	0.909	0.896	0.966	0.948
Random	0.024	0.296	0.165	0.235	0.306	0.451	0.133	0.255	0.172	0.189
Equal	0.894	0.851	0.748	0.714	0.865	0.819	0.913	0.921	0.950	0.951
Dot product	0.917	0.871	0.763	0.729	0.875	0.837	0.927	0.932	0.955	0.955
None	0.963	0.959	0.807	0.786	0.965	0.953	0.854	0.875	0.825	0.860
Grey-scale	0.958	0.965	0.835	0.819	0.955	0.939	0.845	0.851	0.859	0.876
Color jitters	0.955	0.937	0.833	0.804	0.948	0.924	0.844	0.862	0.864	0.880
Rotation	0.975	0.972	0.838	0.814	0.969	0.963	0.849	0.868	0.857	0.876

Table D3: **Impact of the test set size**. We evaluate our method on the ImageNet-R set with different number of test samples.

# samples	3,000	6,000	12,000	18,000	24,000
DoC	0.856	0.848	0.877	0.874	0.874
DoC + Ours	0.873	0.874	0.892	0.895	0.896

D More experiments on variants of vicinal risk proxy

We conduct experiments using different variants of the vicinal risk proxy on the ImageNet-R and ObjectNet datasets. The experimental results in Table D2 show similar observations to those in the main manuscript.

E Impact of test set size

Table D3 presents our method under varying test set sizes using ImageNet-R as an OOD test set. We observe that the performance of all compared methods drops under smaller test sets. Nevertheless, the use of vicinal assessment consistently improves the correlation strength of the baselines under each test set size, demonstrating the effectiveness of our method.

F Vicinal Assessment for Data-centric Unsupervised Evaluation

As discussed in Section 4.4 of the main paper, vicinal assessment technically can be applied in data-centric unsupervised evaluation by measuring scores of a fixed model on various test sets. To evaluate this, we conduct experiments using two models, *Efficientnet-b2* and *Inception-v4*, obtained from the model zoo in Section A.1, on 95 testing sets sourced from the test set pool, ImageNet-C [20]. The experimental results, showcasing the performance the vicinal method under different risk proxies, are presented in Table F4.

Our main observation is that the correlation results obtained using vicinal samples are similar to those relying merely on individual samples. In other words, there is no noticeable improvements as opposed to those model-centric experiments in the main paper. In fact, as illustrated in Fig. 1-4, vicinal proxies are helpful for distinguishing models *w.r.t* their OOD accuracy. Its limited capability in distinguishing hard datasets from easy ones leads to the observations in Table F4.

Table F4: **Effectiveness of vicinal assessment in data-centric unsupervised evaluation.** For each model, the *first* row shows results of baseline risk proxies, while the *second* row gives results of their vicinal assessments. γ and ρ have the same meaning as described in the main paper.

Model	EI		AC		CI		DoC		ATC	
	γ	ρ	γ	ρ	γ	ρ	γ	ρ	γ	ρ
Efficientnet-b2	0.932	0.976	0.987	0.993	0.919	0.965	0.987	0.992	0.933	0.939
	0.942	0.979	0.989	0.994	0.918	0.961	0.989	0.994	0.937	0.938
Inception-V4	0.938	0.970	0.960	0.988	0.931	0.963	0.960	0.988	0.991	0.994
	0.942	0.973	0.964	0.990	0.928	0.960	0.964	0.990	0.993	0.995

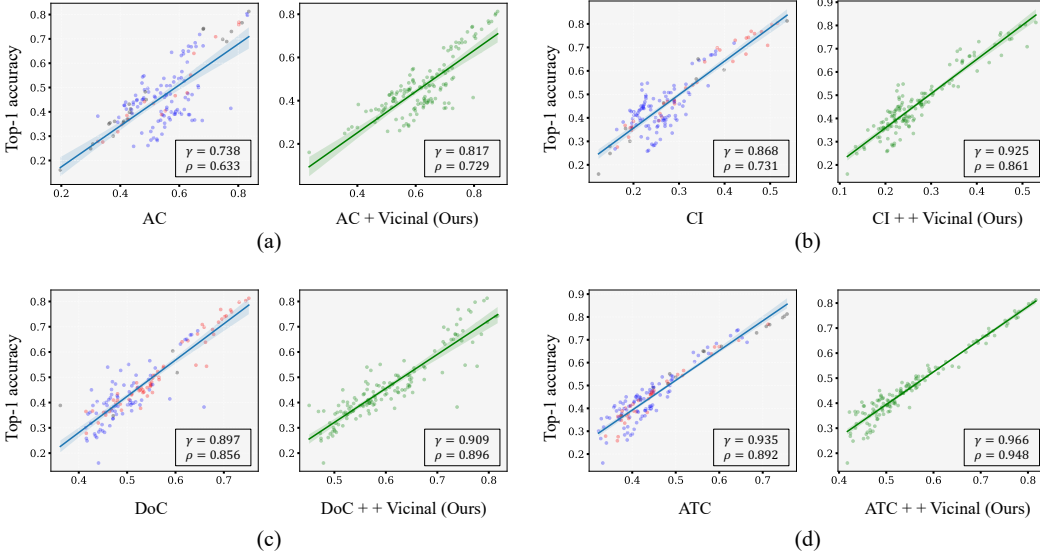


Figure F4: **Correlation between various risk proxies and accuracy on the ImgeNet-R dataset.** All notations in each figure have the same meanings as Fig. 5 of the main ppaer. We observe that proposed vicinal assessment effectively rectifies the risk estimates for the majority of models under various risk proxies.

G More Visualizations of Improved Correlations

In Fig. 5 of the main manuscript, we visualized correlations between effective invariance (EI) and accuracy and the improvement brought by vicinal proxies on the ImgeNet-R and ObjectNet datasets. Here, we present more visualizations, using AC, CI, DOC and ATC proxies. Results are shown in Fig. F4, Fig. F5 and Fig. F6. We observe that generally the proposed vicinal assessment allows more models to get closer to the actual accuracy rank.

Limitation

Our approach faces limitations in deployment environments with severely restricted computational resources, as it necessitates generating predictions from multiple images.

Impact statement

This paper seeks to advance the field of machine learning. There are numerous potential societal benefits from our research, including the development of secure AI, explainable AI, and responsible AI.

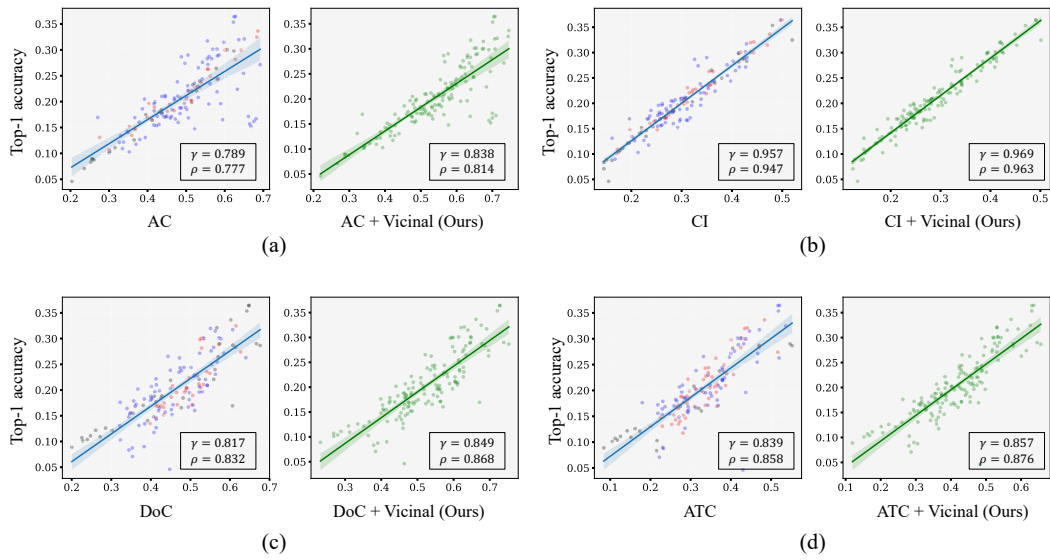


Figure F5: **Correlation between various risk proxies and accuracy on the ObjectNet dataset.** Notations in each figure have the same meanings as Fig. 5 of the main paper. Our observations are similar with those in Fig. F4.

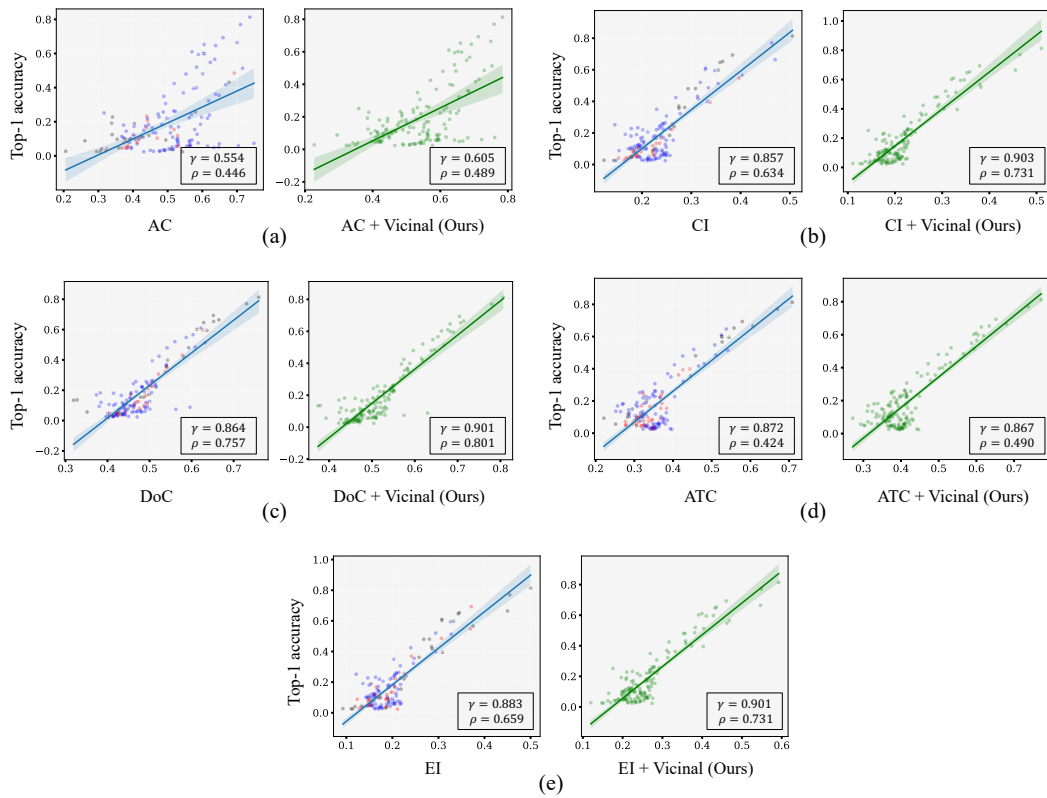


Figure F6: **Correlation between various risk proxies and accuracy on the ImageNet-A dataset.** Notations in each figure have the same meanings as Fig. 5 of the main paper. Our observations are similar with those in Fig. F4 and Fig. F5.